Front. Optoelectron. 2021, 14(2): 211–220
https://doi.org/10.1007/s12200-021-1204-6

RESEARCH ARTICLE

PTX-symmetric metasurfaces for sensing applications

Zhilu YE, Minye YANG, Liang ZHU, Pai-Yen CHEN (✉)

Department of Electrical and Computer Engineering, University of Illinois at Chicago, Chicago, IL 60607, USA

Abstract In this paper, we introduce an ultra-sensitive optical sensing platform based on the parity-time-reciprocal scaling (*PTX*)-symmetric non-Hermitian metasurfaces, which leverage exotic singularities, such as the exceptional point (EP) and the coherent perfect absorber-laser (CPAL) point, to significantly enhance the sensitivity and detectability of photonic sensors. We theoretically studied scattering properties and physical limitations of the *PTX*-symmetric metasurface sensing systems with an asymmetric, unbalanced gain-loss profile. The *PTX*-symmetric metasurfaces can exhibit similar scattering properties as their *PT*-symmetric counterparts at singular points, while achieving a higher sensitivity and a larger modulation depth, possible with the reciprocal-scaling factor (i.e., X transformation). Specifically, with the optimal reciprocal-scaling factor or near-zero phase offset, the proposed *PTX*-symmetric metasurface sensors operating around the EP or CPAL point may achieve an over 100 dB modulation depth, thus paving a promising route toward the detection of small-scale perturbations caused by, for example, molecular, gaseous, and biochemical surface adsorbates.

Keywords parity-time symmetry, exceptional point (EP), laser oscillator, coherent perfect absorber, electromagnetic sensor, radio frequency (RF) and microwave sensing, optical sensing

1 Introduction

The past decades have witnessed the evolution of optical and photonic micro/nano-sensors and the significant contributions they have made for a variety of applications, such as biomedical analysis, non-invasive detection, and environmental monitoring, to name a few [1–8]. With necessity of detecting miniature disturbances, it is desirable to explore and investigate photonic sensors with an extremely high sensitivity and an ultrasmall detection limit. So far, numerous sensing systems have been evaluated toward this goal, such as fiber-optic sensors [9,10], nanowire-based sensors [11,12], tactile sensors based on contact electrification [13]. Along different lines, exceedingly-sensitive sensors with unusual points have recently attracted intense attention [14–21]. Such unusual points are observed in optical and photonic systems described by non-Hermitian Hamiltonians. Possibly the best-known example would be the exceptional points (EPs) typically observed in parity-time (*PT*)-symmetric systems. Interest in *PT*-symmetric systems was originally triggered by developments in quantum mechanics [22], showing that a certain class of non-Hermitian Hamiltonians can exhibit wholly real energy spectra. In electromagnetics, *PT*-symmetric structures, which involve balanced gain and loss components, coalesce two or more eigenvalues at the exceptional points. The indicated EPs have been proven their potential of being utilized for ultra-sensitive sensing systems, thanks to dramatic shifts of eigenfrequencies with respect to external perturbations [14–18,23,24]. Additionally, the coherent perfect absorber-laser (CPAL) point has been found as a self-dual singular point in the *PT*-symmetric system with special relevance for sensing purposes [19–21,25]. At the CPAL point, the eigenvalues of a *PT*-symmetric system will go separate ways, reaching out for zero (CPA state) and infinity (lasing state) individually. Motivated by this CPAL action, we have recently demonstrated a CPAL-locked sensing system in electromagnetic domain, initially kept at CPA state by achieving the designed ratio of complex amplitude between two monochromatic incoming waves [20,21]. A slight disturbance may break the specific condition of initial state, leading a mode switch from CPA to lasing, which results in an unprecedented sensitivity surpassing that of traditional sensors based on Fabry-Perot cavities [20,21].

In spite of these advantages in traditional *PT*-symmetric systems, practical implementations for the ultrasensitive *PT* sensor may face challenges in achieving an exact impedance profile with identical gain/loss pair. To mitigate

Received January 13, 2021; accepted February 21, 2021

E-mail: pychen@uic.edu

these difficulties, we here introduce a thorough research on the generalized sensing platform based on the parity-time-reciprocal scaling (*PTX*)-symmetric metasurfaces operating in the proximity of EP or CPAL point. We will show that an ultrahigh sensitivity and an ultrawide detection range can still be enabled by the reciprocal-scaling operation, first demonstrated in electronic systems [17,26] and later optical metasurface systems [19]. Moreover, the *PTX*-symmetric system can have an eigenspectrum identical to that of the standard *PT*-symmetric system, while allowing unequal gain and loss, and even observation of EP in a fully-passive system [17,19]. More importantly, the scaling operation offers an additional degree of freedom in sensor design, which delicately controls the sensitivity, detection range, and modulation depth. Figure 1(a) shows the two-port transmission line network (TLN) model that can describe the proposed *PTX*-symmetric metasurfaces (which could be realized in different spectra with different techniques). The model consists of a pair of active and passive metasurfaces with surface conductances of $-G/k$ and kG, where k is the reciprocal-scaling factor provided by the X operator. The negative surface conductance may be realized with an active metasurface formed by meta-atoms with photo-excited gain [19,27], as schematically shown in Fig. 1(b). When operating in the vicinity of EP, the metasurface sensing system shows a unique characteristic of unidirectional reflectionless transparency [27,28], which can be disturbed by minute perturbations and hence offers possibility for sensing applications. As for the CPAL point, the proposed sensing system employs lasing state as initial state, of which the sensing functionality is realized by the disappearance of lasing state when an ultrasmall perturbation is applied. Unlike the traditional *PT* sensors utilizing eigenfrequency shifts near the exceptional point, the proposed *PTX* sensors exploits a monochromatic sensing scheme, such that the system is rather insusceptible to the environmental noises, such as phase noise or flicker

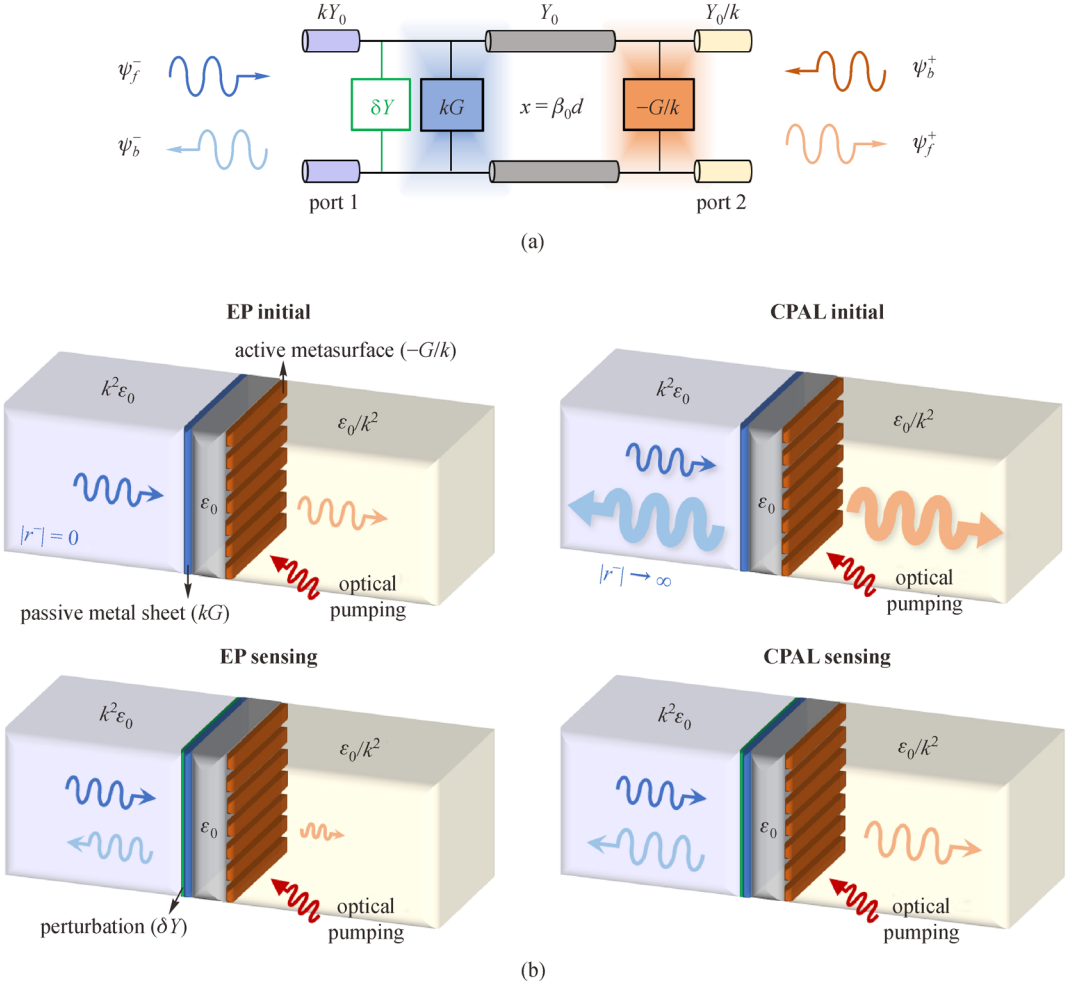

Fig. 1 (a) Equivalent transmission line model for the *PTX*-symmetric sensing system and (b) its practical realization at optical frequencies, where the positive and negative elements can be realized by a passive metal sheet and an optical-pumped active metasurface respectively. In this scheme, two metasurfaces with conductances of kG and $-G/k$ ($G=|-G|=\gamma Y_0$) are separated by an air gap (which is equivalent to a transmission line of characteristic admittance Y_0 and electrical length x). The system is perturbed by a variable admittance δY, which could be a reactive contribution or a conductive one

noise, thereby providing higher signal-to-noise ratio. As shown in the following, besides an ultrahigh sensitivity, the sensing limitation of the EP- or CPAL-based *PTX*-symmetric sensor could be pushed toward infinitesimal by applying the optimum scaling factor or phase offset, consequently providing unprecedentedly excellent sensing performance. Moreover, the introduction of reciprocal-scaling factor k not only allows the adjustment of sensitivity and working range, but also releases the restrictions on the required phase offset in transmission lines (which must be precisely controlled for high sensitivity in standard *PT*-symmetric sensing systems [20]). Compared with the CPAL sensor in Ref. [20] with tight constraints on the complex amplitude ratio between two incident waves, the proposed single port excited scheme also simplifies experimental requirements, thereby offering a preeminent robustness and practical feasibility in optical and photonic sensing.

2 Concept of EP and CPAL actions in *PTX*-symmetric metasurface systems

Figures 1(a) and 1(b) present the schematics and one possible geometry to realize the *PTX*-symmetric metasurface system, comprising a scaled gain-loss pair (i.e., $-G\rightarrow -G/k$, $G\rightarrow kG$) spatially located in two sides of a transmission line with a characteristic admittance Y_0 and an electrical length of $x=\beta_0 d=\pi/2+\delta x$, where β_0, d and δx severally denote the propagation constant, physical length and phase offset of the transmission line segment. In the optical realm, the active and passive metasurfaces, representing the gain and loss elements of the TLN model in Fig. 1(a), must be delicately designed to achieve desired surface impedance required by *PTX*-symmetric conditions. In practice, the passive metasurface can be simply realized with a resistive metal sheet, while an active one can be built using a planar array of photopumped graphene nanoribbons [27]. With a certain value of k, an active metasurface with surface conductance of $-G/k$ can be accomplished by utilizing a suitable photodoping intensity and proper dimension properties of the graphene-nanoribbon array [27]. Moreover, the characteristic impedances of the port 1 (left/loss side) and port 2 (right/gain side) are also scaled by the dimensionless scaling factor k and $1/k$, respectively. Applying this scaling rule in optics domain, the dielectric permittivity of the host substrates should be provided by $k^2\varepsilon_0$ and ε_0/k^2, where ε_0 is the permittivity of free space (Fig. 1(b)). We should note that to meet this criterion, the permittivity ε_{eff} of the host medium is possible to be less than 1 or near zero realized by metamaterials or plasmas at optical frequencies [19]. In this TLN (Fig. 1), it is noticed that the typical *PT*-symmetric system could be regarded as a degenerate case of the *PTX*-scenario with $k=1$. As a result, we can likewise use scattering matrix $\boldsymbol{S}$ to describe input and output waves in the two-port *PTX*-symmetric system with the form of $|\psi_{\text{out}}\rangle=\boldsymbol{S}|\psi_{\text{in}}\rangle$, where $|\psi_{\text{in}}\rangle=(\psi_f^-,\ \psi_b^+)^{\text{T}}$, $|\psi_{\text{out}}\rangle=(\psi_f^+,\ \psi_b^-)^{\text{T}}$, and $\boldsymbol{S}=\begin{pmatrix} t & r^+ \\ r^- & t \end{pmatrix}$. Here, $\psi_f^{\pm}$ and $\psi_b^{\pm}$ sequentially refer to incoming and outgoing waves in the left (–) and right (+) ports. For the *PTX*-symmetric system in Fig. 1, the scattering coefficients in $\boldsymbol{S}$ can be derived using the transfer-matrix method and given by (see Supplementary material for the details)

$$
\begin{aligned}
t &= \frac{\mathrm{i}2k\csc x}{(\gamma^2-2)k+\mathrm{i}(1+k^2+\gamma(k^2-1))\cot x},\\
r^+ &= -\frac{(\gamma+2)\gamma k+\mathrm{i}(\gamma+1)(k^2-1)\cot x}{(\gamma^2-2)k+\mathrm{i}(1+k^2+\gamma(k^2-1))\cot x},\\
r^- &= -\frac{(\gamma-2)\gamma k+\mathrm{i}(\gamma-1)(k^2-1)\cot x}{(\gamma^2-2)k+\mathrm{i}(1+k^2+\gamma(k^2-1))\cot x},
\end{aligned}
\tag{1}
$$

where γ indicates the conductance ratio of the gain/loss component to the characteristic admittance of the transmission line ($\gamma=G/Y_0$). From Eq. (1), it can be seen apparently that the scaling factor k could modify the scattering properties in terms of reflection (r) and transmission (t) coefficients. In addition, we also observe from Eq. (1) that when $x=\pi/2$ (i.e., $\delta x=0$), all scattering coefficients in $\boldsymbol{S}$ and the correlative eigenvalues $\lambda_{\pm}$ become independent of scaling coefficient k, implying that the unbalanced *PTX*-symmetric system shares exactly the same scattering properties as its *PT*-symmetric counterpart with balanced gain and loss. Similarly, the evolution of eigenvalues ($|\lambda_{\pm}|$) of $\boldsymbol{S}$ matrix could be used to characterize the phase transition in this *PTX*-symmetric system. Figure 2 reports the eigenvalues as a function of γ and k for the *PTX*-symmetric system with $\delta x=10^{-3}(\pi/2)$, in which the exact and broken symmetry phases are divided by the exceptional point ($\gamma=2$). More specifically, when $0<\gamma<2$, the *PTX*-symmetric system is in a broken phase where the eigenvalues are non-unimodular (i.e., $\lambda_+=(\lambda_-^*)^{-1}$); when $\gamma>2$, the *PTX*-symmetry system enters the exact phase and the eigenvalues become nondegenerate and unimodular (i.e., $|\lambda_{\pm}|=1$). In addition, it is observed that a CPAL point induced by self-dual spectral singularity occurs in the broken symmetry phase ($\gamma=\sqrt{2}$), where the *PTX*-symmetric electromagnetic system possesses zero and infinity eigenvalues simultaneously, representing the CPA and lasing states respectively.

3 EP-based *PTX*-symmetric metasurface sensing systems

To characterize scattering properties of the *PTX*-symmetric metasurfaces, we introduce the output coefficient Θ

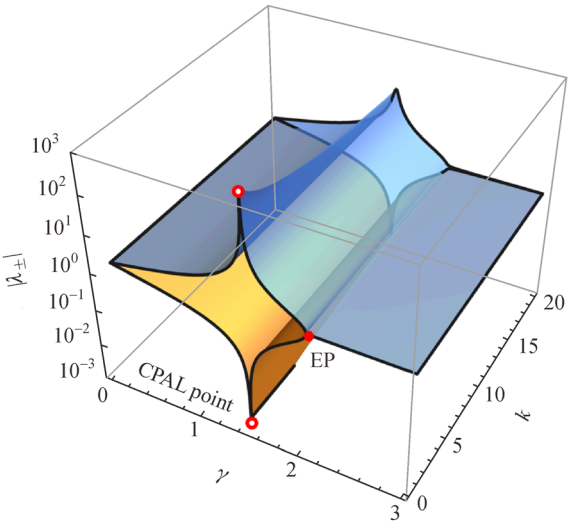

Fig. 2 Evolution of eigenvalues as a function of γ and k for the *PTX* system in Fig. 1; here, $\delta x = 10^{-3}(\pi/2)$ and $\delta Y = 0$. We should note that if $x = \pi/2$ (or $\delta x = 0$), the eigenvalues are unaffected by scaling factor k. The system can be divided into the exact symmetry phase ($\gamma > 2$) and the broken *PTX*-symmetry phase ($\gamma < 2$), with a discontinuous phase transition at the exceptional point ($\gamma = 2$). In the broken phase, two eigenvalues approach infinity (lasing state) and zero (CPA state) at the CPAL point ($\gamma = \sqrt{2}$)

defined as the total output power divided by the input power, which could be written as

$$\Theta = \frac{k|\psi_b^-|^2 + |\psi_f^+|^2/k}{k|\psi_f^-|^2 + |\psi_b^+|^2/k}. \tag{2}$$

For the system operating at the EP ($\gamma = 2$), a distinctive property of unidirectional reflectionless may be obtained (i.e., $|r^-| = 0$ according to Eq. (1)), and its sensing functionality may be realized by drastically breaking this reflection response with a tiny perturbation. On that account, we consider here the EP-locked sensing scenario with left (–) port (port 1) excitation and only the reflected wave ψ_b^- is taken into account for the output factor in Eq. (2), i.e., $\psi_f^- = 1, \psi_b^+ = \psi_f^+ = 0$. By applying a small-scale perturbation $\nu = \delta Y/Y_0$ to the loss side (which could be either resistive or reactive), the initial state of unidirectional reflectionless may be disturbed and the associated output coefficient can be approximately expressed as (see Supplementary material for the detailed derivations of output coefficients)

$$\Theta(\nu) \approx \frac{\nu^2}{4k^2} + \mathrm{O}(\nu^3). \tag{3}$$

From Eq. (3), we find that the slope of the output coefficient versus ν^2, which is a measurement of sensitivity, is governed by the dimensionless parameter $1/(4k^2)$ and unrelated to the phase offset δx. In addition, the output factor Θ is limited with upper and lower bounds of 1 and $(k^2-1)^2\delta x^2/(4k^2)$ respectively, from which it is noted that the initial or minimum value of Θ could approach zero when k is set to 1 or $\delta x = 0$. Under this specific circumstance, the sensing limitation (i.e., lower detection bound) may be remarkably infinitesimal and the sensing system accordingly achieves its maximal working range. Figure 3(a) plots the output coefficient under the effect of a minuscule disturbance ν with different phase offset δx (k is kept as constant 2), where the approximate output factor (dashed line) obtained from Eq. (3) matches

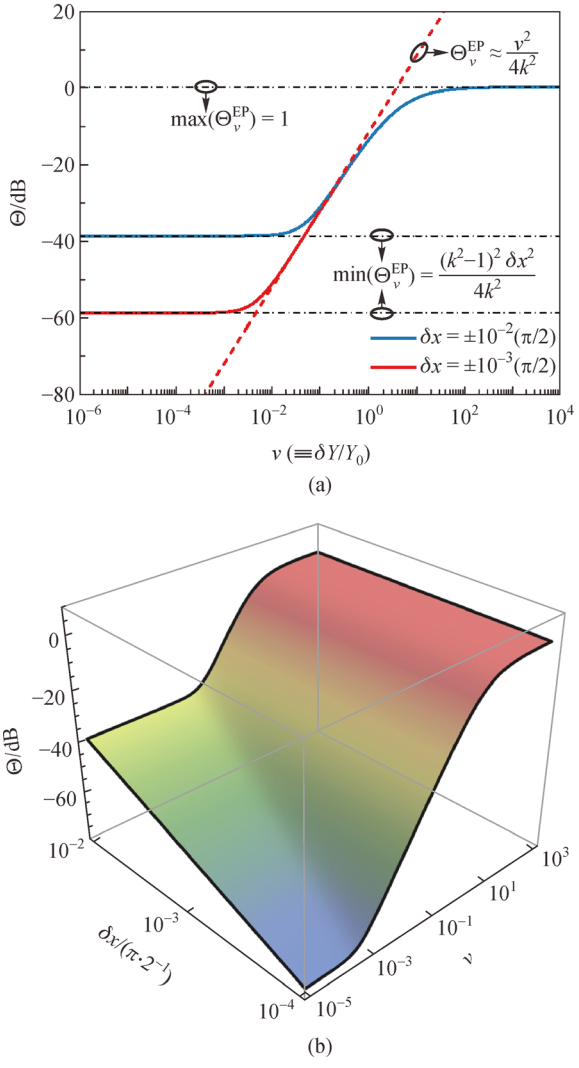

Fig. 3 (a) Output coefficient of the *PTX*-symmetric EP sensor in Fig. 1 under small perturbations $\nu = \delta Y/Y_0$; here, $\gamma = 2$ and $k = 2$. Dashed line is the approximate results obtained from Eq. (3). We note that $\Theta(\nu)$ is not affected by the sign of δx. (b) Contours of output coefficient as a function of ν and δx. The lower bound of output coefficient (or detection limit) can be minimized as $(\delta x)^2$ decreases

the accurate value (solid lines) truly well in the operation range. From Fig. 3(a), it is evidently observed that such unidirectional reflectionless property at the EP, indeed, enables photonic sensors with an extremely high sensitivity. Additionally, its sensing limitation and working range could be modulated through the adjustment of phase offset δx. The contours of Θ as a function of ν and δx are shown in Fig. 3(b), which further illustrate that the lower bound of Θ or detection limit could be minimized by decreasing δx. Particularly, a large modulation depth up to 70 dB may be obtained with a phase offset $\delta x \sim 10^{-4}(\pi/2)$.

Next, the influence of scaling factor k on output intensity is also studied and the results are depicted in Figs. 4(a) and 4(b); here $\delta x = 10^{-3}(\pi/2)$. As expected, the scaling factor

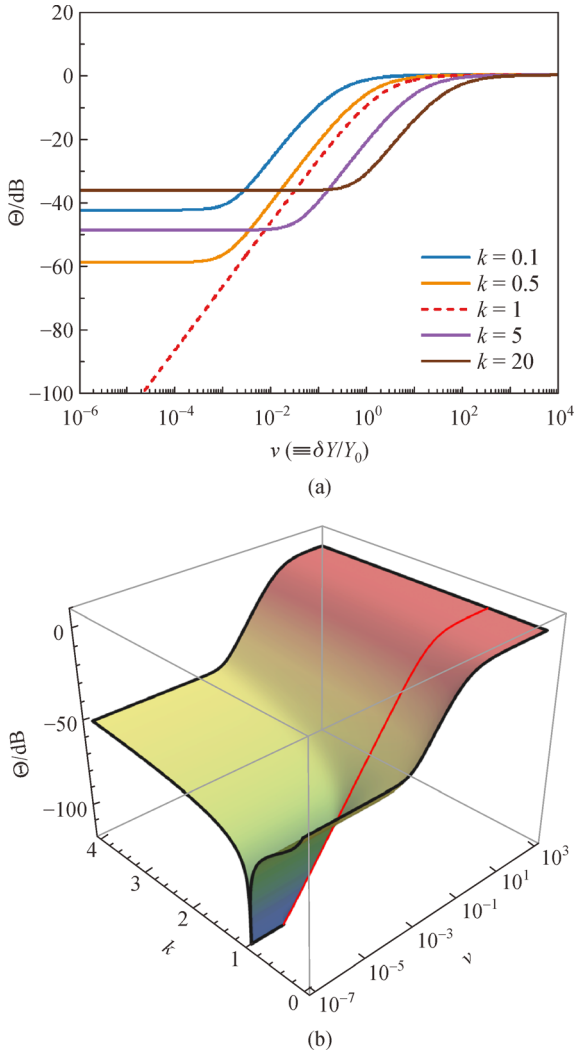

Fig. 4 (a) Output coefficient $\Theta(\nu)$ of the *PTX*-symmetric EP sensor with different scaling factor k; here, $\gamma = 2$ and $\delta x = 10^{-3}(\pi/2)$. (b) Contours of output intensity as a function of ν and k. The slope of $\Theta(\nu^2)$, or sensitivity, and working range can be tuned by modifying scaling factor. When $k = 1$, the lower detection limit is approaching zero, leading to infinitesimal sensing limitation and the topmost operation range

k has the potential for tuning sensitivity and working range. To be more precise, sensitivity which appears as the slope of $\Theta(\nu^2)$ can be improved by reducing k, and a scaling factor k near 1 could help the *PTX*-symmetric EP sensor achieve an initial condition of near-zero output coefficient Θ, thus realizing an ultrasmall sensing limitation and the maximum working range. Also, the optimum condition $k = 1$ releases the restrictions on the phase offset, so as to offer the EP-locked sensing system excellent tolerance to errors in the assembly and fabrication of transmission lines.

4 CPAL-based *PTX*-symmetric metasurface sensing systems

In this section, we study the effect of perturbations on the output coefficient of the *PTX*-symmetric metasurface system locked to the CPAL point. We note that under the CPAL condition, i.e., $x = \pi/2$ and $\gamma = \sqrt{2}$, the lasing mode could always be obtained with single port excitation (i.e., $\psi_f^- = 1$, $\psi_b^+ = 0$ for port 1 incidence while $\psi_f^- = 0$, $\psi_b^+ = 1$ for wave coming from right side, i.e., port 2) [19]. It is worthwhile mentioning that the proposed single port excited *PTX*-symmetric CPAL sensing system has hardly any restrictions on input signals which are necessarily required for achieving the initial CPA mode in Ref. [20]. However, it could still accomplish a superior sensitivity owing to the rapid amplitude dropping of the output coefficient at design frequency when applying ultrasmall-scale perturbations. Let us first analyze the performance of the CPAL-locked *PTX*-symmetric sensor with left-incident wave (loss side) excited by port 1. Considering a small resistive or reactive perturbation $\nu = \delta Y/Y_0$ ($\nu \ll 1$) applied on the loss component and solely detecting the reflected wave ψ_b^-, the output factor could be approximated as (see Supplementary material for the detailed derivations of output coefficients)

$$\Theta(\nu) \approx \frac{4k^2}{\nu^2} + \mathrm{O}(\nu^3), \tag{4}$$

which accurately predicts the output coefficient affected by small values of ν, as shown in Fig. 5(a). It is evidently seen from Eq. (4) that sensitivity, or the slope of $\Theta(\nu^{-2})$, is dominated by the factor $4k^2$ and rather independent of the phase offset δx, revealing that sensitivity of the CPAL-locked sensor can be modified by tuning the scaling factor k. In point of fact, the suggested *PTX*-symmetric CPAL sensing system offers eminent sensitivity, which is also tunable and may be ameliorated by choosing large scaling coefficient k appropriately (Fig. 6).

In addition, the detection limit and working range of the proposed *PTX* system could be described by physical bounds of the output intensity. For this port 1 excited *PTX*-symmetric CPAL metasurface sensor, the initial or maximum value of output intensity could be expressed

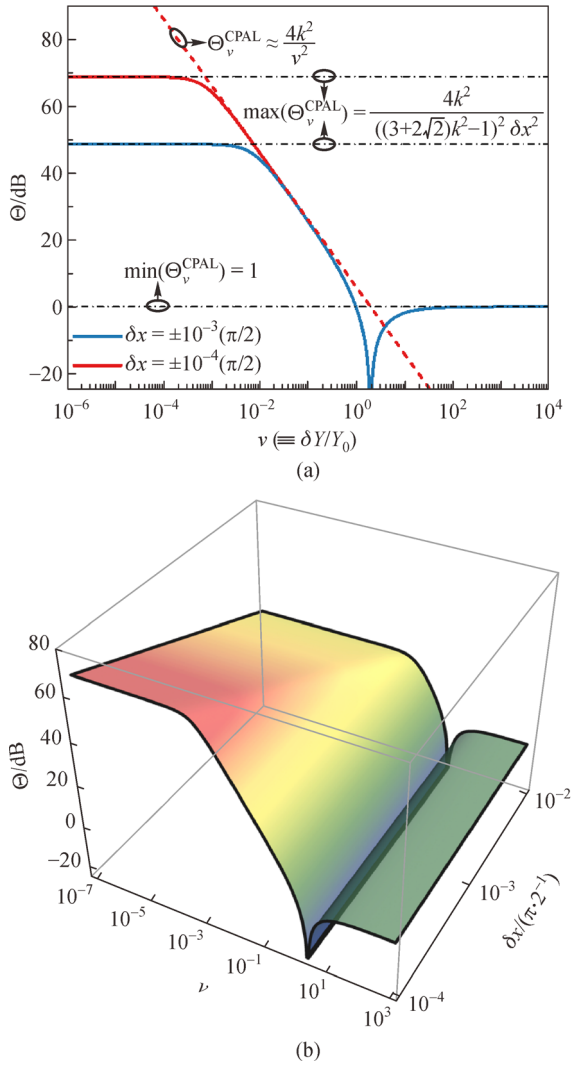

Fig. 5 (a) Output coefficient of the *PTX*-symmetric CPAL sensor in Fig. 1 under tiny perturbations $\nu = \delta Y/Y_0$; here, $\gamma = \sqrt{2}$ and $k = 1$. Dashed line is the approximate results obtained from Eq. (4). (b) Contours of output coefficient as a function of ν and δx. The upper bound (or maximum value) of the output coefficient can be greatly enhanced as $(\delta x)^2$ decreases

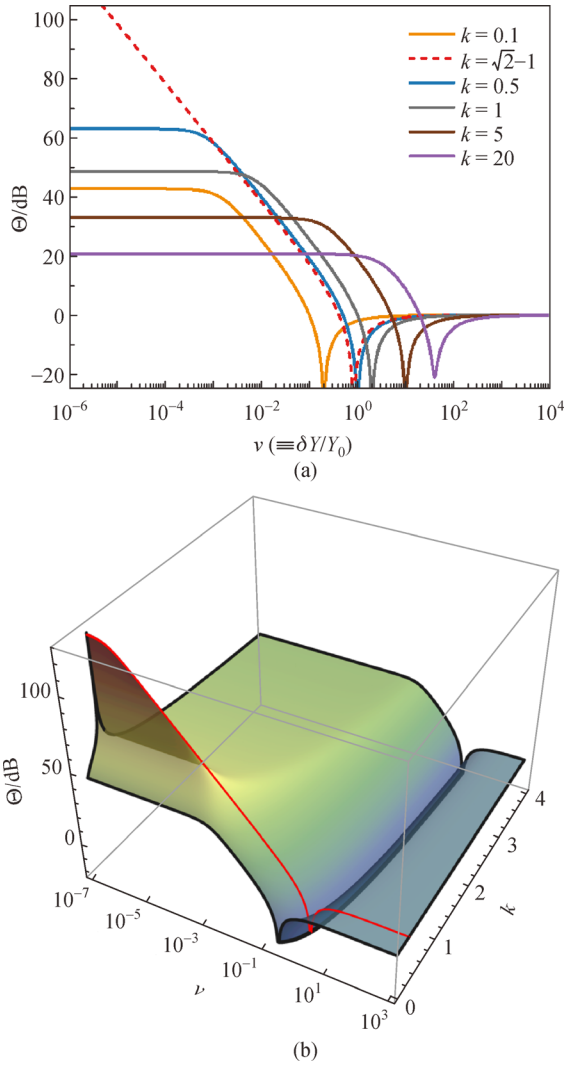

Fig. 6 (a) Output coefficient $\Theta(\nu)$ of the *PTX*-symmetric CPAL sensor with different scaling factor k; here, $\gamma = \sqrt{2}$ and $\delta x = 10^{-3}(\pi/2)$. (b) Contours of output intensity as a function of ν and k. When $k = \sqrt{2}-1$, $\max(\Theta_\nu)$ is pushed toward infinity, conforming to near-zero sensing limitation

by $\max(\Theta_\nu) = \dfrac{4(17-12\sqrt{2})k^2}{(-3+2\sqrt{2}+k^2)^2\delta x^2}$. If the perturbation is fairly massive, the output coefficient will converge to its lower limitation: $\min(\Theta_\nu) = 1$. Interestingly, the denominator of $\max(\Theta_\nu)$ becomes zero when $\delta x = 0$ or $k = \sqrt{2}-1$, showing that the initial (maximum) value of output coefficient may theoretically achieve infinity. As a result, the sensing limitation, directly linked with $\max(\Theta_\nu)$, may be significantly enhanced and even pushed toward infinitesimal with a tiny δx or a scaling factor near $\sqrt{2}-1$. Figure 5 compares the metasurface sensing systems based on different phase offset δx (here $k = 1$), in response to a small perturbation ν, which proves that the reduction of phase offset from $\delta x \sim 10^{-2}(\pi/2)$ to $\delta x \sim 10^{-4}(\pi/2)$ could result in a significant enhancement of sensing limitation and modulation depth. The output coefficients as a function of k and ν are depicted in Fig. 6 with a phase offset $\delta x = 10^{-3}(\pi/2)$, illustrating that the scaling factor k offers the possibility of adjustable sensing limitation and tunable working range. It should be noted that, although $k = \sqrt{2}-1$ is not capable of bringing the largest sensitivity, it can still be regarded as the optimal scaling factor since it offers decent sensitivity with the lowest detection limit and the maximum working range. In practice, the phase offset may be minimized by utilizing advanced complimentary metal-oxide-semiconductor

Table 1 Performance of *PTX*-symmetric CPAL sensor

excitation/detection port	approximate $\Theta(\nu)$	upper bound	lower bound
port 1/port 1	$\frac{4k^2}{\nu^2}$	$\frac{4(17-12\sqrt{2})k^2}{(-3+2\sqrt{2}+k^2)^2\delta x^2}$	1
port 1/port 1&2	$\frac{4(3+2\sqrt{2}+k^2)}{\nu^2}$	$\frac{4(17-12\sqrt{2})(3+2\sqrt{2}+k^2)}{(-3+2\sqrt{2}+k^2)^2\delta x^2}$	1
port 2/port 2	$\frac{4(17+12\sqrt{2})k^2}{\nu^2}$	$\frac{4k^2}{(-3+2\sqrt{2}+k^2)^2\delta x^2}$	$17+12\sqrt{2}$
port 2/port 1&2	$\frac{4k^2(17+12\sqrt{2}+(3+2\sqrt{2})k^2)}{\nu^2}$	$\frac{4k^2+4(3-2\sqrt{2})k^4}{(-3+2\sqrt{2}+k^2)^2\delta x^2}$	$17+12\sqrt{2}$

(CMOS) photonics and integrated optics technologies. On the other hand, the optimal value of k could be readily realized, for instance, through careful design of the active/passive metasurface with desired surface conductance values.

Here, we also fully investigate the cases where the *PTX*-symmetric CPAL sensing system (a) is excited with left-incident wave (port 1) and both reflection and transmission are detected for output intensity; (b) is excited with right-incident wave (port 2) and only reflected wave is considered; (c) is excited with right-incident wave (port 2) and both reflection and transmission are counted for output coefficient. For all three cases, the output factors Θ under perturbation $\nu = \delta Y / Y_0$ are listed in Table 1, where we perceive the similarities between these circumstances and the aforementioned sensing scheme (i.e., left-port excitation and single reflection detection); these include adjustable sensitivity and tunable working range provided by k, and near-zero sensing limitation accomplished by a minimized δx or a scaling factor $k = \sqrt{2}-1$. Noticeably, the lower bound of output intensity in case (a) is 1 whereas those in cases (b) and (c) are $17+12\sqrt{2}$, showing that sensing systems with incident wave coming from the loss side possess broader working range and larger modulation depth in contrast to the gain-side excitation scenarios. Since two-port detection requires more complicated experimentation platform without producing preferable performance, the single port excited sensing system with left-incident wave and reflection detection is concluded as the most distinguished sensing scheme for its manageable feature and marvelous sensing performance.

5 Conclusions

We have thoroughly analyzed the monochromatic *PTX*-symmetric metasurfaces for sensing applications, which may take advantages of drastic changes in optical scattering properties nearby the EP and CPAL point. We have theoretically shown that the output coefficient of the proposed sensing scheme is extremely sensitive to external perturbations. Further, our results have shown that the phase offset δx related to the separation distance between two metasurfaces is responsible for the sensing limitation and detection range, while the reciprocal-scaling factor k associated with the X transformation determines the sensitivity of the system. Through a systematic study, we have found out that the optimal scaling factor ($k = 1$ for the EP-based sensor and $k = \sqrt{2}-1$ for the CPAL-based sensor) may achieve the maximum detection range (for both lower and upper bounds). The proposed *PTX*-symmetric metasurface sensors with advantages of low profile and ultrahigh sensitivity may open a new avenue of the next-generation high-performance optical and photonic sensors in different spectral ranges.

References

1. Rodriguez S, Ollmar S, Waqar M, Rusu A. A batteryless sensor ASIC for implantable bio-impedance applications. IEEE Transactions on Biomedical Circuits and Systems, 2016, 10(3): 533–544
2. Yvanoff M, Venkataraman J. A feasibility study of tissue characterization using LC sensors. IEEE Transactions on Antennas and Propagation, 2009, 57(4): 885–893
3. Tan Q, Luo T, Xiong J, Kang H, Ji X, Zhang Y, Yang M, Wang X, Xue C, Liu J, Zhang W. A harsh environment-oriented wireless passive temperature sensor realized by LTCC technology. Sensors (Basel, Switzerland), 2014, 14(3): 4154–4166
4. Huang H, Chen P Y, Hung C H, Gharpurey R, Akinwande D. A zero power harmonic transponder sensor for ubiquitous wireless μL liquid-volume monitoring. Scientific Reports, 2016, 6(1): 18795
5. Chen L Y, Tee B C K, Chortos A L, Schwartz G, Tse V, Lipomi D J, Wong H S, McConnell M V, Bao Z. Continuous wireless pressure monitoring and mapping with ultra-small passive sensors for health monitoring and critical care. Nature Communications, 2014, 5(1): 5028
6. Chen P, Rodger D C, Saati S, Humayun M S, Tai Y. Microfabricated implantable parylene-based wireless passive intraocular pressure sensors. Journal of Microelectromechanical Systems, 2008, 17(6): 1342–1351
7. Chen P, Saati S, Varma R, Humayun M S, Tai Y. Wireless intraocular pressure sensing using microfabricated minimally invasive flexible-coiled LC sensor implant. Journal of Microelec-

tromechanical Systems, 2010, 19(4): 721–734
8. Nopper R, Niekrawietz R, Reindl L. Wireless readout of passive LC sensors. IEEE Transactions on Instrumentation and Measurement, 2010, 59(9): 2450–2457
9. Lopez-Higuera J M, Cobo L R, Incera A Q, Cobo A. Fiber optic sensors in structural health monitoring. Journal of Lightwave Technology, 2011, 29(4): 587–608
10. Lee B H, Kim Y H, Park K S, Eom J B, Kim M J, Rho B S, Choi H Y. Interferometric fiber optic sensors. Sensors (Basel, Switzerland), 2012, 12(3): 2467–2486
11. Liao L, Lu H B, Li J C, Liu C, Fu D J, Liu Y L. The sensitivity of gas sensor based on single ZnO nanowire modulated by helium ion radiation. Applied Physics Letters, 2007, 91: 173110
12. Wanekaya A K, Chen W, Myung N V, Mulchandani A. Nanowire-based electrochemical biosensors. Electroanalysis, 2006, 18(6): 533–550
13. Zhu G, Yang W Q, Zhang T, Jing Q, Chen J, Zhou Y S, Bai P, Wang Z L. Self-powered, ultrasensitive, flexible tactile sensors based on contact electrification. Nano Letters, 2014, 14(6): 3208–3213
14. Xiao Z, Li H, Kottos T, Alù A. Enhanced sensing and nondegraded thermal noise performance based on PT-symmetric electronic circuits with a sixth-order exceptional point. Physical Review Letters, 2019, 123(21): 213901
15. Chen P Y, El-Ganainy R. Exceptional points enhance wireless readout. Nature Electronics, 2019, 2(8): 323–324
16. Hodaei H, Hassan A U, Wittek S, Garcia-Gracia H, El-Ganainy R, Christodoulides D N, Khajavikhan M. Enhanced sensitivity at higher-order exceptional points. Nature, 2017, 548(7666): 187–191
17. Chen P Y, Sakhdari M, Hajizadegan M, Cui Q, Cheng M M C, El-Ganainy R, Alù A. Generalized parity–time symmetry condition for enhanced sensor telemetry. Nature Electronics, 2018, 1(5): 297–304
18. Dong Z, Li Z, Yang F, Qiu C W, Ho J S. Sensitive readout of implantable microsensors using a wireless system locked to an exceptional point. Nature Electronics, 2019, 2(8): 335–342
19. Sakhdari M, Estakhri N M, Bagci H, Chen P Y. Low-threshold lasing and coherent perfect absorption in generalized PT-symmetric optical structures. Physical Review Applied, 2018, 10(2): 024030
20. Farhat M, Yang M, Ye Z, Chen P Y. PT-symmetric absorber-laser enables electromagnetic sensors with unprecedented sensitivity. ACS Photonics, 2020, 7(8): 2080–2088
21. Yang M, Ye Z, Farhat M, Chen P Y. Enhanced radio-frequency sensors based on a self-dual emitter-absorber. Physical Review Applied, 2021, 15(1): 014026
22. Bender C M, Boettcher S. Real spectra in non-Hermitian Hamiltonians having PT symmetry. Physical Review Letters, 1998, 80(24): 5243–5246
23. Sakhdari M, Hajizadegan M, Zhong Q, Christodoulides D N, El-Ganainy R, Chen P Y. Experimental observation of PT symmetry breaking near divergent exceptional points. Physical Review Letters, 2019, 123(19): 193901
24. Chen W, Kaya Özdemir Ş, Zhao G, Wiersig J, Yang L. Exceptional points enhance sensing in an optical microcavity. Nature, 2017, 548 (7666): 192–196 PMID:28796206
25. Longhi S. PT-symmetric laser absorber. Physical Review A, 2010, 82(3): 031801
26. Ye Z, Farhat M, Chen P Y. Tunability and switching of Fano and Lorentz resonances in *PTX*-symmetric electronic systems. Applied Physics Letters, 2020, 117(3): 031101
27. Chen P Y, Jung J. PT symmetry and singularity-enhanced sensing based on photoexcited graphene metasurfaces. Physical Review Applied, 2016, 5(6): 064018
28. Sakhdari M, Farhat M, Chen P Y. PT-symmetric metasurfaces: wave manipulation and sensing using singular points. New Journal of Physics, 2017, 19(6): 065002

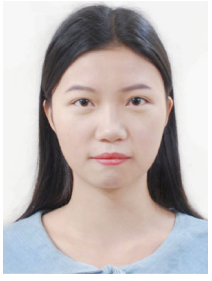

Zhilu Ye received the B.S degree in Microelectronics from Huazhong University of Science and Technology, China, in 2018, and the master's degree in Electrical Engineering from Arizona State University, USA, in 2019. Since then, she has been with University of Illinois at Chicago, USA, where she is pursing the Ph.D. degree. Her research interest includes RF and microwave sensors, wireless communication and wearable electronics.

Minye Yang completed the bachelor's degree in Optical and Electronic Information from Huazhong University of Science and Technology, China, in 2018, and received the M.Sc. degree in Electrical Engineering from Wayne State University, USA, in 2019. He is currently pursuing the Ph.D. degree in Electrical Engineering at University of Illinois at Chicago, USA. His research focuses on ultrasensitive electromagnetic sensors, RF/microwave circuits.

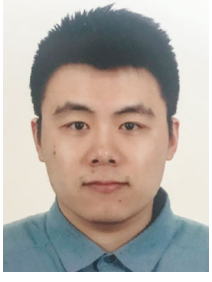

Liang Zhu received the M.Sc. degree in Optics from Sun Yat-sen University, China, in 2015. He is currently pursuing the Ph.D. degree in Electrical Engineering at University of Illinois at Chicago, USA. His research mainly focuses on RF/microwave antennas and circuits, energy harvesting platforms and wireless sensors.

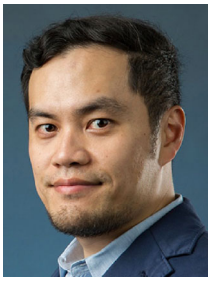

Pai-Yen Chen (S'09, M'13, SM'17) is an Associate Professor in Department of Electrical and Computer Engineering at University of Illinois at Chicago, USA. He received his Ph.D. degree from University of Texas at Austin, USA, in 2013. He has been involved in multidisciplinary research on applied electromagnetics, RF/microwave antennas and circuits, wireless micro/nano-sensors and integrated systems, as well as nanoelectromagnetism in plasmonics and nanophotonics. He has received quite a few prestigious awards, including National Science Foundation (NSF) CAREER Award, IEEE Sensors Council Young Professional Award, IEEE Raj Mittra Travel Grant (RMTG) Award, SPIE Rising

Researcher Award, ACES Early Career Award, PIERS Young Professional Award, Young Scientist Awards from URSI General Assembly and URSI Commission B: Electromagnetics, Air Force Research Laboratory Faculty Fellowship, National Argonne Laboratory Director's Fellowship, College of Engineering Faculty Research Excellence Award, Donald Harrington Fellowship, United Microelectronics Corporation Scholarship, and quite a few student paper awards and travel grants from major IEEE conferences, including the USNC-URSI Ernest K. Smith Student Paper Award. He currently serves as Associate Editor of *IEEE Sensors Journal*, *IEEE Journal of Radio Frequency Identification* (IEEE JRFID), *IEEE Journal of Electromagnetics, RF and Microwaves in Medicine and Biology* (IEEE-JERM), and Guest Editor of several international journals. He was a former Associate Editor of *Applied Electromagnetics*.

Supplementary material

A. Scattering and transfer matrices

The transfer matrix $\boldsymbol{M}$ of the *PTX*-symmetric two-port transmission line network at the CPAL point in Fig. 1 could be written as

$$\boldsymbol{M}=\begin{pmatrix} M_{11} & M_{12} \\ M_{21} & M_{22} \end{pmatrix},$$

where

$$\begin{aligned} M_{11} &= \frac{(1+k^2-\gamma(k^2-1))\cos x+\mathrm{i}(\gamma^2-2)k\sin x}{2k}, \\ M_{12} &= \frac{-(\gamma+1)(k^2-1)\cos x+\mathrm{i}(\gamma+2)\gamma k\sin x}{2k}, \\ M_{21} &= \frac{(\gamma-1)(k^2-1)\cos x-\mathrm{i}(\gamma-2)\gamma k\sin x}{2k}, \\ M_{22} &= \frac{(1+k^2+\gamma(k^2-1))\cos x-\mathrm{i}(\gamma^2-2)k\sin x}{2k}, \end{aligned} \tag{S1}$$

and $\gamma=G/Y_0$ which describes the conductance ratio of the gain/loss component to the characteristic admittance of the transmission line.

The scattering matrix $\boldsymbol{S}$ can be expressed as $\boldsymbol{S}=\begin{pmatrix} t & r^+ \\ r^- & t \end{pmatrix}$, the transmission ($t$) and reflection ($r$) coefficients for left (–) and right (+) incidences can be derived according to the transfer matrix elements: $r^-=-M_{21}/M_{22}$, $r^+=M_{12}/M_{22}$ and $t^+=t^-=t=1/M_{22}$. The CPAL point will occur when $\gamma=\sqrt{2}$ and $x=\pi/2$ (i.e., at design frequency). If γ is set to be $\sqrt{2}$, the eigenvalues can be written as a function of frequency:

$$\lambda_{\pm}=\frac{2k\pm\sqrt{4k^2+(1-6k^2+k^4)\cos^2(\omega\pi/(2\omega_0))}}{(1-\sqrt{2}+(1+\sqrt{2})k^2)\cos(\omega\pi/(2\omega_0))}, \tag{S2}$$

where ω_0 is the design angular frequency. Additionally, if $x=\pi/2$, the eigenvalues can be expressed as

$$\lambda_{\pm}=\frac{2\mathrm{i}\pm\gamma\sqrt{\gamma^2-4}}{\gamma^2-2}. \tag{S3}$$

It is evidently seen from Eqs. (1) and (S3) that the $\boldsymbol{S}$ matrix and the corresponding eigenvalues are independent of the scaling factor k at design frequency ($x=\pi/2$).

B. Expressions for output coefficients

When the system in Fig. 1(a) is operating at the EP ($\gamma=2$) and $x=\pi/2+\delta x$, left (–) incident wave is considered and the reflected wave is counted for the output factor. With a small-scale perturbation $\nu=\delta Y/Y_0$ applied to the loss side, the output coefficient can be written as

$$\begin{aligned} \Theta(\nu) &= \frac{\nu^2+(k(k+\nu)-1)^2\tan^2(\delta x)}{(2k+\nu)^2+(k(3k+\nu)-1)^2\tan^2(\delta x)} \\ &\approx \frac{\nu^2}{4k^2}+\frac{(k^2-1)^2\delta x^2}{4k^2}+\mathrm{O}(\nu^3),\ \text{if}\ \nu\ll 1 \\ &\approx \frac{\nu^2}{4k^2}. \end{aligned} \tag{S4}$$

For the system working at the CPAL point ($\gamma=\sqrt{2}$ and $x=\pi/2+\delta x$), a tiny resistive or reactive perturbation $\nu=\delta Y/Y_0$ ($\nu\ll 1$) is introduced to the loss side. Considering left-incident wave excitation and solely detecting the reflected wave ψ_b^-, the output factor can be expressed as

$$\begin{aligned} \Theta(\nu) &= \frac{(3-2\sqrt{2})(\nu-2k)^2+((1-\sqrt{2})(1-k^2)+k\nu)^2\tan^2(\delta x)}{(3-2\sqrt{2})\nu^2+(1-\sqrt{2}+(1+\sqrt{2})k^2+k\nu)^2\tan^2(\delta x)} \\ &\approx \frac{4k^2}{\nu^2}-\frac{4k}{\nu}+1+\mathrm{O}(\nu^3),\quad \text{if}\ \nu\ll 1 \\ &\approx \frac{4k^2}{\nu^2}. \end{aligned} \tag{S5}$$

With left-incident wave excitation and both the reflected and transmitted wave detected, the output factor can be expressed as

$$\begin{aligned}\Theta(\nu) &= \frac{(3-2\sqrt{2})(\nu-2k)^2 + 4\sec^2(\delta x) + (1-\sqrt{2}+(\sqrt{2}-1)k^2+k\nu)^2\tan^2(\delta x)}{(3-2\sqrt{2})\nu^2 + (1-\sqrt{2}+(1+\sqrt{2})k^2+k\nu)\tan^2(\delta x)} \\ &\approx \frac{4(3+2\sqrt{2}+k^2)}{\nu^2} - \frac{4k}{\nu} + 1 + \mathrm{O}(\nu^3),\ \text{if}\ \nu \ll 1 \\ &\approx \frac{4(3+2\sqrt{2}+k^2)}{\nu^2}. \end{aligned} \tag{S6}$$

Similarly, when the system is excited with incident wave coming from gain side and only reflection is considered, the output coefficient can be written as

$$\begin{aligned}\Theta_\nu &= \frac{(3+2\sqrt{2})(\nu+2k)^2 + ((1+\sqrt{2})(1-k^2)-k\nu)^2\tan^2(\delta x)}{(3-2\sqrt{2})\nu^2 + (1-\sqrt{2}+(1+\sqrt{2})k^2+k\nu)^2\tan^2(\delta x)} \\ &\approx \frac{4(17+12\sqrt{2})k^2}{\nu^2} + \frac{4(17+12\sqrt{2})k}{\nu} + 17 + 12\sqrt{2} + \mathrm{O}(\nu^3), \quad \text{if}\ \nu \ll 1 \\ &\approx \frac{4(17+12\sqrt{2})k^2}{\nu^2}. \end{aligned} \tag{S7}$$

If right-incident wave is considered and both reflection and transmission are counted, the output coefficient can be derived as

$$\begin{aligned}\Theta_\nu &= \frac{(3+2\sqrt{2})(\nu+2k)^2 + 4k^4\sec^2(\delta x) + ((1+\sqrt{2})(1-k^2)-k\nu)^2\tan^2(\delta x)}{(3-2\sqrt{2})\nu^2 + (1-\sqrt{2}+(1+\sqrt{2})k^2+k\nu)^2\tan^2(\delta x)} \\ &\approx \frac{4k^2(17+12\sqrt{2}+(3+2\sqrt{2})k^2)}{\nu^2} + \frac{4(17+12\sqrt{2})k}{\nu} + 17 + 12\sqrt{2} + \mathrm{O}(\nu^3), \quad \text{if}\ \nu \ll 1 \\ &\approx \frac{4k^2(17+12\sqrt{2}+(3+2\sqrt{2})k^2)}{\nu^2}. \end{aligned} \tag{S8}$$